

Electron Correlation and Pairing States in Superconductors without Inversion Symmetry

Satoshi Fujimoto*

Department of Physics, Kyoto University, Kyoto 606-8502, Japan

(Received September 12, 2018)

This article is a pedagogical review of theoretical studies of noncentrosymmetric superconductors with particular emphasis on the role played by electron correlation, which is important for heavy fermion systems. We survey unique properties of parity-violated superconductivity such as the admixture of spin singlet and triplet states, unusual paramagnetism, large Pauli limiting fields, magnetoelectric effects, the helical vortex phase, and the anomalous Hall effect. It is pointed out that these remarkable features are strengthened by a strong electron correlation effect, and thus are prominent in heavy fermion superconductors without inversion symmetry. We also discuss possible pairing states realized in the heavy fermion system CePt₃Si.

KEYWORDS: superconductivity, heavy fermion, inversion symmetry, electron correlation

1. Introduction

In all superconductors, the symmetries of systems such as time-reversal symmetry and inversion symmetry impose important constraint on pairing states. For instance, when a system has an inversion center, Cooper pairs are classified into a spin-singlet state or a spin-triplet state according to parity. Conversely, in the case without inversion symmetry, in which an asymmetric potential gradient yields a spin-orbit (SO) interaction that breaks parity, the admixture of a spin singlet state and a spin triplet state is possible, and also, various exotic electromagnetic properties may result. Such parity-violated superconductivity is the main topic of this article. Pioneering theoretical studies on this subject were initiated by Bulaevskii et al. decades ago, and developed by Edelstein in 1989.¹⁻⁴ Edelstein pointed out that, in addition to the singlet-triplet mixing of pairing states, the parity-breaking SO interaction also gives rise to unusual electromagnetism such as van-Vleck-like spin susceptibility analogous to van-Vleck orbital susceptibility, and magnetoelectric effects, i.e., supercurrent induced by the Zeeman field, and conversely, magnetization induced by supercurrent flow. The latter effects are due to the nontrivial coupling between the spin and charge degrees of freedom raised by a parity-breaking SO interaction. These intriguing phenomena were also investigated in more detail by Gor'kov and Rashba, and Yip.^{5,6} However, experimental tests on these interesting theoretical predictions in real materials have not been performed for decades since the first prediction made by Edelstein.¹

In 2004, Bauer et al. discovered a bulk superconductor without inversion symmetry, CePt₃Si,⁷ and stimulated more extensive experimental and theoretical studies on this subject.⁸⁻²⁷ In particular, the ETH group and Agterberg revealed some novel aspects of electromagnetic properties such as large Pauli limiting fields, and a possible realization of the helical vortex state in magnetic fields.^{15,19} The helical vortex state is a kind of the Fulde-Ferrel state in which Cooper pairs have a center of

mass momentum, and the phase of the order parameter is spatially modulated. This Fulde-Ferrel-like state was also independently predicted by Samokhin on the basis of the general GL theory with strong SO coupling.¹⁶

After this breakthrough, other novel heavy fermion superconductors without inversion symmetry such as UIr, CeRhSi₃, and CeIrSi₃ have been discovered.²⁸⁻³⁰ Also, in non-*f*-electron systems, new noncentrosymmetric superconductors such as Cd₂Re₂O₇, Li₂Pd₃B, and Li₂Pt₃B have been discovered.³¹⁻³⁴ An intriguing feature of these systems is that according to LDA calculations and de Haas-van Alphen experiments, the SO splitting of the Fermi surfaces is much larger than the superconducting gap.^{17,35-37} For instance, in the case of CePt₃Si, the magnitude of the SO splitting is nearly equal to 10 percent of the Fermi energy.^{17,35} This large SO splitting indicates the important role of parity violation in these superconductors.

In this article, we survey theoretical studies of noncentrosymmetric superconductors with particular emphasis on the role played by electron correlation effects and the application to heavy fermion systems. In heavy fermion systems where *f*-electrons are itinerant, there exists a strong spherically-symmetric SO interaction in addition to the parity-breaking SO interaction. Thus, we need to clarify the relation between these different types of SO interaction. The parity-breaking SO interaction due to an asymmetric potential gradient ∇V is generally expressed as $(\mathbf{k} \times \nabla V) \cdot \boldsymbol{\sigma}$, where \mathbf{k} is the momentum, and $\boldsymbol{\sigma}$ is the Pauli matrix. This SO interaction is expressed in terms of electron spins. In the case of CePt₃Si, because of the strong symmetric SO interaction, the ground state of the *f*-electron level is the Γ_7 Kramers doublet, the basis of which is,⁹

$$\begin{aligned} |a\rangle &= \sqrt{5/6}|5/2\rangle - \sqrt{1/6}| -3/2\rangle, \\ |\bar{a}\rangle &= \sqrt{5/6}| -5/2\rangle - \sqrt{1/6}|3/2\rangle. \end{aligned} \quad (1)$$

Transforming the basis of spin to the basis $|a\rangle, |\bar{a}\rangle$, we find that the parity-breaking SO interaction is rewritten as $(5/12)(\mathbf{k} \times \nabla V) \cdot \boldsymbol{\sigma}$, where the Pauli matrix $\boldsymbol{\sigma}$

*E-mail address: fuji@scphys.kyoto-u.ac.jp

is defined in the pseudospin space spanned by $|a\rangle$, $|\bar{a}\rangle$. That is, the matrix structure is not affected, and only the constant prefactor is changed. Thus, even in the case of heavy fermion systems, as long as the Bloch states of f -electrons are labeled by pseudospins that constitute the Kramers doublet, we can use the same expression of the parity-breaking SO interaction as that for electron spins. Throughout this paper, when we consider heavy fermion systems, we use the terms “spin singlet state” and “spin triplet state” to indicate the pseudospin singlet state and the pseudospin triplet state, respectively. In the case that upper levels of f -electrons are not negligible, we need a more elaborate treatment of the parity-breaking SO interaction.

The organization of this paper is as follows: In §2, we present the microscopic description of the superconducting state without inversion symmetry which takes electron correlation effects into account. This section is a bit technical. Readers who are not interested in the technical details may proceed to the next sections. In §3, we argue the pairing state on the basis of the BCS weak-coupling approximation, focusing on the admixture of spin singlet and triplet states. In §4, we study unique electromagnetic properties of noncentrosymmetric superconductors. In §5, we provide a discussion on possible pairing states realized in CePt₃Si. In §6, we give concluding remarks.

2. Fermi Liquid Theory for Superconductors without Inversion Symmetry

In this section, we present the basic formulation for the BCS theory of noncentrosymmetric superconductors, which includes electron correlation effects as the Fermi liquid corrections.^{22,27} We are mainly concerned with electromagnetic properties. As is shown below, unique features of magnetism in inversion-symmetry-broken systems appear as a result of paramagnetic effects rather than diamagnetic effects. Thus we take into account the Zeeman coupling with an external magnetic field $\mathbf{H} = (H_x, H_y, H_z)$, neglecting the orbital diamagnetic effect for a while. Thus, our analysis is based on the following simple Hamiltonian,

$$\mathcal{H} = \mathcal{H}_0 + \mathcal{H}_{\text{SO}} + \mathcal{H}_{\text{Zeeman}}, \quad (2)$$

$$\mathcal{H}_0 = \sum_{k,\sigma} \varepsilon_k c_k^\dagger c_k + U \sum_i n_{\uparrow i} n_{\downarrow i}, \quad (3)$$

$$\mathcal{H}_{\text{SO}} = \alpha \sum_k c_k^\dagger \mathbf{L}_0(k) \cdot \boldsymbol{\sigma} c_k, \quad (4)$$

$$\mathcal{H}_{\text{Zeeman}} = \sum_k c_k^\dagger \mu_B \boldsymbol{\sigma} \cdot \mathbf{H} c_k. \quad (5)$$

where $c_k^\dagger = (c_{\uparrow k}^\dagger, c_{\downarrow k}^\dagger)$ is the two-component spinor field for an electron with the spin \uparrow, \downarrow , and the momentum k . $n_{\sigma i} = c_{\sigma i}^\dagger c_{\sigma i}$ is the number density operator at the site i . The components of $\boldsymbol{\sigma} = (\sigma_x, \sigma_y, \sigma_z)$ are the Pauli matrix. The vector $\mathbf{L}_0(k) = (\mathcal{L}_{0x}, \mathcal{L}_{0y}, \mathcal{L}_{0z})$ in the spin-orbit interaction term \mathcal{H}_{SO} obeys $\mathbf{L}_0(-k) = -\mathbf{L}_0(k)$, breaking inversion symmetry. The explicit form of $\mathbf{L}_0(k)$ is determined by details of the crystal structure. In the case of the tetragonal structure with an asymmetric potential gradient along the z -axis, $\mathbf{L}_0(k) = (k_y, -k_x, 0)$

for a small k , which is the Rashba interaction.³⁸ In the case of cubic structures with the point group symmetry T , such as the zinc-blende, $\mathbf{L}_0(k) = (k_x(k_y^2 - k_z^2), k_y(k_z^2 - k_x^2), k_z(k_x^2 - k_y^2))$, which is related to the Dresselhaus interaction.³⁹⁻⁴¹ For simplicity, we assume that the g -factor is equal to 2, and spin $s = 1/2$. As a matter of fact, for heavy fermion systems the g -factor may generally be different from 2 because of the strong symmetric SO interaction.

Electron correlation effects, which are important for heavy fermion systems, are incorporated by on-site Coulomb repulsion U . We also assume that, in addition to the on-site repulsion, there is an effective pairing interaction with an angular momentum $\ell \geq 1$, which may stem from the on-site Coulomb interaction in (2) or from any other factors not included in the Hamiltonian (2).

To calculate physical quantities microscopically, we utilize the single-particle Green function, the inverse of which is, in the conventional Nambu representation, defined as

$$\hat{\mathcal{G}}^{-1}(p) = \begin{pmatrix} i\varepsilon_n - \hat{H}(p) & -\hat{\Delta}(p) \\ -\hat{\Delta}^\dagger(p) & i\varepsilon_n + \hat{H}^t(-p) \end{pmatrix}, \quad (6)$$

where $p = (i\varepsilon_n, \mathbf{k})$ and

$$\hat{H}(p) = \varepsilon_k - \mu + \alpha \mathbf{L}_0(k) \cdot \boldsymbol{\sigma} + \hat{\Sigma}(p) + \mu_B \boldsymbol{\sigma} \cdot \mathbf{H}, \quad (7)$$

with μ being the chemical potential. The self-energy matrix $\hat{\Sigma}$ consists of both diagonal and off-diagonal components, and expressed as

$$\begin{aligned} \hat{\Sigma} &= \begin{pmatrix} \Sigma_{\uparrow\uparrow}(p) & \Sigma_{\uparrow\downarrow}(p) \\ \Sigma_{\downarrow\uparrow}(p) & \Sigma_{\downarrow\downarrow}(p) \end{pmatrix} \\ &= \Sigma_0 + \boldsymbol{\Sigma} \cdot \boldsymbol{\sigma}, \end{aligned} \quad (8)$$

where $\boldsymbol{\Sigma} = (\Sigma_x, \Sigma_y, \Sigma_z)$ with $\Sigma_0 = (\Sigma_{\uparrow\uparrow} + \Sigma_{\downarrow\downarrow})/2$, $\Sigma_x = (\Sigma_{\downarrow\uparrow} + \Sigma_{\uparrow\downarrow})/2$, $\Sigma_y = (\Sigma_{\downarrow\uparrow} - \Sigma_{\uparrow\downarrow})/2i$, and $\Sigma_z = (\Sigma_{\uparrow\uparrow} - \Sigma_{\downarrow\downarrow})/2$.

The SO interaction $\alpha \mathbf{L}_0(k) \cdot \boldsymbol{\sigma}$ splits the Fermi surface into two parts as shown in Fig. 1. The SO split two bands are derived by diagonalizing $i\varepsilon_n - \hat{H}(p)$ and $i\varepsilon_n + \hat{H}^t(-p)$ in $\hat{\mathcal{G}}^{-1}(p)$. The diagonalization is a bit tricky because $\boldsymbol{\Sigma}(p)$ is generally non-Hermitian. In the absence of the magnetic field, we can verify that $\Sigma_x(p)$ and $\Sigma_y(p)$ are real quantities, and thus $\boldsymbol{\Sigma}(p)$ is Hermitian.²⁷ Also, as long as the linear response against the magnetic field is concerned, the imaginary part of $\Sigma_x(p)$ and $\Sigma_y(p)$ are negligible compared to the real parts even for $\mathbf{H} \neq 0$. Then, the diagonalization is achieved by using the unitary transformation $\hat{\mathcal{A}}(p)\hat{\mathcal{G}}^{-1}(p)\hat{\mathcal{A}}^\dagger(p)$ with

$$\hat{\mathcal{A}}(p) = \begin{pmatrix} \hat{U}(p) & 0 \\ 0 & \hat{U}^{t\dagger}(-p) \end{pmatrix}, \quad (9)$$

$$\hat{U}(p) = \begin{pmatrix} \xi_+(p) & \xi_-(p)\eta_-(p) \\ -\xi_-(p)\eta_+(p) & \xi_+(p) \end{pmatrix}, \quad (10)$$

$$\xi_{\pm}(p) = \frac{1}{\sqrt{2}} \left[1 \pm \frac{\mathcal{L}_z(p)}{\|\mathcal{L}(p)\|} \right]^{\frac{1}{2}}, \quad (11)$$

$$\eta_{\pm}(p) = \frac{\mathcal{L}_x(p) \pm i\mathcal{L}_y(p)}{\sqrt{\mathcal{L}_x(p)^2 + \mathcal{L}_y(p)^2}}. \quad (12)$$

Here,

$$\mathcal{L}(p) = (\mathcal{L}_x(p), \mathcal{L}_y(p), \mathcal{L}_z(p)) = \mathcal{L}_0(k) - \frac{\mu_B}{\alpha} \mathbf{H} + \frac{1}{\alpha} \Sigma(p). \quad (13)$$

$$\text{and } \|\mathcal{L}(p)\| = \sqrt{\mathcal{L}_x^2 + \mathcal{L}_y^2 + \mathcal{L}_z^2}.$$

In the absence of the magnetic field $\mathbf{H} = 0$, the superconducting gap function $\hat{\Delta}(p)$ in eq. (6) is also diagonalized by $\hat{\mathcal{A}}$ if and only if the gap function has the form,^{1,15,22}

$$\hat{\Delta}(p) = \Delta_s(k) i\sigma_y + \Delta_t(k) \mathcal{L}(p) \cdot \sigma i\sigma_y \quad (14)$$

That is, when the \mathbf{d} -vector of the triplet gap satisfies $\mathbf{d} \propto \mathcal{L}(p)$, there is no Cooper pair between electrons on the different Fermi surfaces splitted by the SO interaction. Conversely, unless $\mathbf{d} \propto \mathcal{L}(p)$, pairing correlation between the SO splitted two bands is induced, which yields pair-breaking effects. (see Fig.1.) According to weak-coupling calculations performed by Frigeri et al.,¹⁵ the \mathbf{d} -vector parallel to $\mathcal{L}(p)$ gives the highest T_c , as long as the pairing interaction stabilizes the gap function with the same momentum dependence as that of $\mathcal{L}(p)$. In general, a finite magnetic field gives rise to pairing correlations between the different Fermi surfaces, and thus the gap $\hat{\Delta}(p)$ can not be diagonalized by $\hat{\mathcal{A}}$. However, within the linear response theory, which is adequate for the following argument, the correlation between the different Fermi surfaces is negligible, and the inverse of eq.(6) is given by,

$$\hat{G}(p) = \begin{pmatrix} \hat{G}(p) & \hat{F}(p) \\ \hat{F}^\dagger(p) & -\hat{G}^t(-p) \end{pmatrix}, \quad (15)$$

where

$$\hat{G}(p) = \sum_{\tau=\pm 1} \frac{1 + \tau \hat{\mathcal{L}}(p) \cdot \sigma}{2} G_\tau(p), \quad (16)$$

$$\hat{F}(p) = \sum_{\tau=\pm 1} \frac{1 + \tau \hat{\mathcal{L}}(p) \cdot \sigma}{2} i\sigma_y F_\tau(p), \quad (17)$$

and

$$G_\tau(p) = \frac{z_{k\tau} (i\varepsilon + \varepsilon_{k\tau}^*)}{(i\varepsilon + i\gamma_{k\tau} \text{sgn}\varepsilon)^2 - E_{k\tau}^2}, \quad (18)$$

$$F_\tau(p) = \frac{z_{k\tau} \Delta_{k\tau}}{(i\varepsilon + i\gamma_{k\tau} \text{sgn}\varepsilon)^2 - E_{k\tau}^2}. \quad (19)$$

Here, $E_{k\tau} = \sqrt{\varepsilon_{k\tau}^{*2} + \Delta_{k\tau}^2}$, $\Delta_{k\tau} = z_{k\tau} \tilde{\Delta}_{k\tau}$ with

$$\tilde{\Delta}_{k\tau} = \Delta_s(k) + \tau |\mathcal{L}(k)| \Delta_t(k), \quad (20)$$

and $\varepsilon_{k\tau}^*$ is the quasiparticle energy determined by using

$$\varepsilon_{k\tau}^* + \mu - \varepsilon_k - \Sigma_0(\varepsilon_k^*, \mathbf{k}) - \tau \alpha \|\mathcal{L}(\varepsilon_{k\tau}^*, \mathbf{k})\| = 0. \quad (21)$$

$\gamma_{k\tau}$ is the quasi-particle damping given by

$$\gamma_{k\tau} = z_{k\tau} (\text{Im} \Sigma_0^R(\varepsilon, \mathbf{k}) + \alpha \text{Re} \hat{\mathcal{L}}^R \cdot \text{Im} \Sigma^R(\varepsilon, \mathbf{k}))|_{\varepsilon \rightarrow i\varepsilon_n}, \quad (22)$$

where $\text{Re} \hat{\mathcal{L}}^R = \text{Re} \mathcal{L}^R(\varepsilon, \mathbf{k}) / |\text{Re} \mathcal{L}^R(\varepsilon, \mathbf{k})|$ and quantities with the superscript R indicate retarded functions obtained by the analytic continuation $i\varepsilon_n \rightarrow \varepsilon + i\delta$ ($\delta > 0$). The mass renormalization factor $z_{k\tau}$ is defined as

$$z_{k\tau} = \left[1 - \frac{\partial \Sigma_0(p)}{\partial(i\varepsilon_n)} - \tau \alpha \frac{\partial \|\mathcal{L}(p)\|}{\partial(i\varepsilon_n)} \right]^{-1} \Big|_{i\varepsilon_n \rightarrow \varepsilon_{k\tau}^*}. \quad (23)$$

In the derivation of the above equations, we assumed that the quasiparticle approximation is applicable. As will be seen in the following, when the SO splitting is much larger than the superconducting gap, some electromagnetic properties are dominated by electrons far from the Fermi surfaces. In such cases, the quasiparticle approximation is not generally applicable, and one needs to take into account the full-energy dependence of the self-energy.

3. Pairing State — Admixture of Spin Singlet State and Spin Triplet State

One of the most remarkable features of noncentrosymmetric superconductors is the admixture of spin singlet and spin triplet states.^{1,5,15} This phenomenon is conceptually understood as follows. When a system has a crystal structure without an inversion center, an asymmetric potential gradient ∇V exists, causing the spin-orbit (SO) interaction $(\mathbf{k} \times \nabla V) \cdot \sigma$, which breaks parity as well as spin inversion symmetry. The asymmetric SO interaction splits the Fermi surfaces into two parts. We show a simple example in Fig.1 in the case of $\nabla V \parallel \mathbf{n} \equiv (001)$, which corresponds to the Rashba-type SO interaction. In Fig. 1, the spin quantization axis is parallel to $\mathbf{k}_F \times \nabla V$. Then, on one of the SO splitted Fermi surfaces, a Cooper pair consists of an electron with the momentum k and spin \rightarrow , and an electron with the momentum $-k$ and spin \leftarrow ; i.e. $|k \rightarrow\rangle | -k \leftarrow\rangle$. Since the counterpart of this state, $|\leftarrow\rangle |\rightarrow\rangle$, is formed on the other Fermi surface, the superposition of these states is impossible. The pairing state $|\rightarrow\rangle |\leftarrow\rangle$ is an admixture of a spin singlet state and a spin triplet state with an in-plane spin projection equal to zero, i.e., $|\rightarrow\rangle |\leftarrow\rangle = [(|\rightarrow\rangle |\leftarrow\rangle - |\leftarrow\rangle |\rightarrow\rangle) + (|\rightarrow\rangle |\leftarrow\rangle + |\leftarrow\rangle |\rightarrow\rangle)]/2$. This means that for the spin quantization axis parallel to the z -axis, the spin triplet component has the nonzero spin projection, $S_z = \pm 1$. (see Fig.2.) More precisely, the spin part of the triplet pairs is determined by the parity-breaking SO interaction, ensuring that the pairing correlation between different Fermi surfaces, which yields pair breaking effects, is suppressed, as pointed out in the previous section.

To obtain further insight into the pairing state, we switch to a microscopic argument based on the BCS theory. The superconducting gap function $\Delta_{\alpha\beta}$ and the transition temperature are determined by the self-consistent gap equation,

$$\Delta_{\alpha\beta} = T \sum_{n,p} \text{Tr}[\hat{\Gamma}^{\alpha\beta}(p, p') \hat{F}(p')], \quad (24)$$

where $\hat{F}(p)$ is the anomalous Green function defined by eq. (17). We have introduced the four-point vertex function matrix $\{\hat{\Gamma}^{\alpha\beta}(p, p')\}_{\gamma\delta}$. This pairing interaction consists of the parity-conserving part $\hat{\Gamma}_{\text{con}}$ and the parity-nonconserving part $\hat{\Gamma}_{\text{noncon}}$, i.e., $\hat{\Gamma} = \hat{\Gamma}_{\text{con}} + \hat{\Gamma}_{\text{noncon}}$. The former can be decomposed into spin singlet and triplet channels. Let us assume the following form of the pairing interaction.

$$\begin{aligned} \{\hat{\Gamma}_{\text{con}}^{\alpha\beta}(p, p')\}_{\gamma\delta} &= \Gamma_{\text{con}}^{(s)}(p, p') i(\sigma_y)_{\alpha\beta} i(\sigma_y)_{\gamma\delta} \\ &+ \Gamma_{\text{con}}^{(t)}(p, p') \mathcal{L}(p) \cdot (\sigma i\sigma_y)_{\alpha\beta} \mathcal{L}(p') \cdot (\sigma i\sigma_y)_{\gamma\delta} \end{aligned} \quad (25)$$

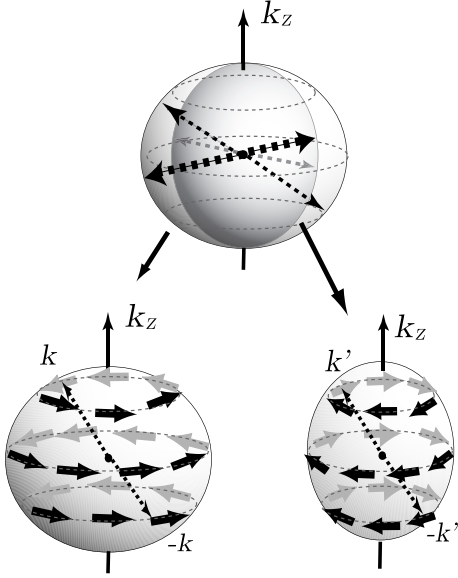


Fig. 1. Two Fermi surfaces splitted by the Rashba SO interaction. On each Fermi surface, spins are parallel to $\mathbf{k} \times \nabla V$, and have a definite eigen value of $(\mathbf{k} \times \mathbf{n}) \cdot \boldsymbol{\sigma}/|\mathbf{k}|$; i.e. +1 or -1. When $\mathbf{d} \propto \mathcal{L}_0(\mathbf{k})$, Cooper pairs are formed on each Fermi surfaces (black and gray dotted thin arrows). When the \mathbf{d} -vector is not parallel to $\mathcal{L}_0(\mathbf{k})$, the pairing correlation between the different Fermi surfaces exists (black dotted thick arrows), which gives rise to pair-breaking effects.

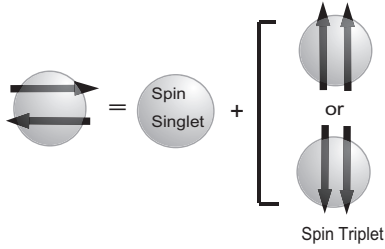


Fig. 2. Schematic picture of parity-violated Cooper pairs. The left-hand side represents the Cooper pair $|\rightarrow\rangle|\leftarrow\rangle$ with the spin quantization axis parallel to $\mathbf{k} \times \mathbf{n}$. The right-hand side represents the sum of a spin singlet state and a spin triplet state with $S_z = \pm 1$ for the spin quantization axis parallel to the z -axis.

The form of the triplet part is chosen to prevent the pairing between the different Fermi surfaces due to the mismatch between the \mathbf{d} -vector and the momentum dependence of the SO interaction, as pointed out in the previous section.^{1, 15, 22} The four-point vertices $\Gamma_{\text{con}}^{(\nu)}$ ($\nu = s, t$) are expanded in terms of the basis of the irreducible representations of the point group of the system. Generally, the parity-nonconserving part $\hat{\Gamma}_{\text{noncon}}$ is nonzero, and expressed as

$$\{\hat{\Gamma}_{\text{noncon}}^{\alpha\beta}(p, p')\}_{\gamma\delta} = \Gamma^{(st)}(p, p')i(\sigma_y)_{\alpha\beta}\mathcal{L}(p') \cdot (\boldsymbol{\sigma}i\sigma_y)_{\gamma\delta}\Delta_t = 0.002498, \Delta_s = 0.0001468. \quad (26)$$

$$+\Gamma^{(ts)}(p, p')\mathcal{L}(p) \cdot (\boldsymbol{\sigma}i\sigma_y)_{\alpha\beta}i(\sigma_y)_{\gamma\delta}.$$

$\Gamma^{(st)}$ and $\Gamma^{(ts)}$ are also classified in accordance with the irreducible representations. The highest T_c is achieved by $\Gamma^{(\nu)}(p, p')$ ($\nu = s, t, st, ts$) which belongs to a unique irreducible representation, provided that there is no accidental degeneracy. Thus, $\Delta_s(p)$ and $\Delta_t(p)$ in eq.(14) are

expressed by the same basis function of the irreducible representation. The superconducting state realized is the mixture of the spin singlet and triplet states.^{1, 5} In this case, the triplet pairing state should be in a higher angular momentum state than the singlet pairing state, and the possible pairing state is $s + p$ or $d + f$ or $g + h$, and so forth.

To examine to what extent the admixture is realized, we carry out a simple model calculation of the transition temperature T_c and the gap function Δ . We consider a two-dimensional model with an isotropic Fermi surface and the Rashba interaction $\mathcal{L}_0(\mathbf{k}) = (k_y, -k_x, 0)$. We also assume the existence of a pairing interaction in the s -wave and the p -wave channels expressed as

$$V_{\text{pair}}(k, k') = u_s c_{k\uparrow}^\dagger c_{-k\downarrow}^\dagger c_{-k'\downarrow} c_{k'\uparrow} + u_p [(i\hat{k}_+)(i\hat{k}'_+)c_{k\uparrow}^\dagger c_{-k\uparrow}^\dagger c_{-k'\uparrow} c_{k'\uparrow} + (i\hat{k}_-)(i\hat{k}'_-)c_{k\downarrow}^\dagger c_{-k\downarrow}^\dagger c_{-k'\downarrow} c_{k'\downarrow}], \quad (27)$$

with $\hat{k}_\pm = (k_x \pm ik_y)/|\mathbf{k}|$, and ignore any other interaction processes. Then, the weak-coupling BCS gap equation is

$$\Delta_\tau = \sum_{\tau'=\pm} g_{\tau\tau'} \sum_k \Delta_{\tau'} \frac{\tanh(\frac{E_{k\tau'}}{2T})}{2E_{k\tau'}}, \quad (\tau = \pm) \quad (28)$$

where $\Delta_\tau = \Delta_s + \tau\Delta_t$ with Δ_s and Δ_t the gap functions for the spin singlet and spin triplet states, respectively. $g_{\tau\tau'} = -(u_s + \tau\tau'u_t)/2$ and $E_{k\tau} = \sqrt{\varepsilon_{k\tau}^2 + \Delta_\tau^2}$. The transition temperature T_c is easily calculated by using the linearized gap equation. In Fig.3(a), we show the results of T_c plotted as a function of u_s for the attractive p -wave interaction with $u_p = -0.15E_F$, and $E_{\text{SO}}/E_F = 0.1$ or $E_{\text{SO}}/E_F = 0.05$ with E_{SO} the magnitude of the SO splitting. For the attractive s -wave interaction $u_s < 0$, T_c increases, as $|u_s|$ changes from 0 to $|u_p|$, indicating that the s -wave pairing mixes with the p -wave pairing cooperatively. It is noted that for $u_s \approx u_p$, T_c is substantially increased by the admixture. On the other hand, for the repulsive s -wave interaction $u_s > 0$, T_c is decreased by the admixture. The decrease in T_c is at most of order E_{SO}/E_F for all positive values of u_s including an extreme case of $u_s/|u_p| \rightarrow \infty$. To observe the admixture more directly, we show in Fig.3(b) the calculated results of the gap function for the spin triplet pair Δ_t and the spin singlet pair Δ_s in the case of $E_{\text{SO}}/E_F = 0.1$ at zero temperature. For the attractive $u_s < 0$, the mixed s -wave gap grows significantly, as $|u_s|$ increases. The maximum ratio of Δ_s/Δ_t for $u_p < u_s < 0$ is nearly equal to 0.32. In contrast to the substantial admixture for $u_s < 0$, Δ_s/Δ_p is at most of order $E_{\text{SO}}/E_F = 0.1$ in the case of the repulsive $u_s > 0$. We found that even in the limit of $u_s \rightarrow \infty$, there exists a solution of the gap equation: $\Delta_t = 0.002498$, $\Delta_s = 0.0001468$. Thus, even when there is a strong on-site Coulomb repulsion, as in the case of heavy fermion systems, the $s + p$ wave state may be possible, as long as E_{SO}/E_F is sufficiently smaller than unity.

In the above argument, it is postulated that the \mathbf{d} -vector of the triplet pairing can be compatible with the momentum dependence of the SO interaction $\mathcal{L}_0(\mathbf{k})$ to prevent the pairing between the different Fermi surfaces.

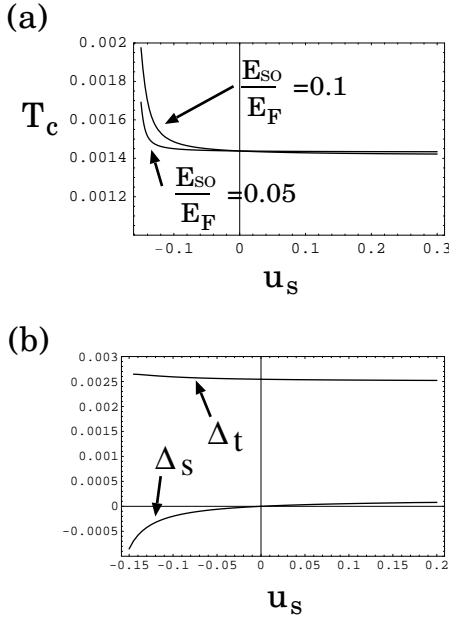


Fig. 3. (a) T_c vs u_s . (b) Δ_s and Δ_t vs u_s at zero temperature for $E_{SO}/E_F = 0.1$.

However, this condition is not generally guaranteed. It may be possible that for some specific electronic structures, the strongest attractive interaction in the triplet channel has a momentum dependence inconsistent with $\mathcal{L}_0(k)$, and thus the gap function $\hat{\Delta}(k)$ cannot be diagonalized by the unitary transformation $\hat{U}(k)\hat{\Delta}(k)\hat{U}^\dagger(-k)$. The realization of this pairing state depends on the competition between the strength of the attractive interaction and the pair-breaking effect caused by the pairing between the different Fermi surfaces.

4. Electromagnetic Properties

4.1 Paramagnetism

The parity-breaking SO interaction yields unique paramagnetic properties. For example, the transition between the two SO splitted Fermi surfaces gives rise to a van-Vleck-like spin susceptibility in addition to the Pauli spin susceptibility.^{1, 5, 15, 22} The van-Vleck-like term is analogous to the conventional van-Vleck orbital susceptibility. However, there are some crucial differences between them, as argued below. An important feature of the van-Vleck-like term is that when the SO splitting $E_{SO} = \alpha|\mathcal{L}|$ is much larger than the superconducting gap Δ , as in the case of CePt₃Si, CeRhSi₃, and CeIrSi₃, this term is not strongly affected by superconducting transition,^{1, 5, 15} in contrast to the Pauli term which decreases below T_c for spin singlet pairing states.

Here, we first consider the Rashba SO interaction relevant to tetragonal systems, $\mathcal{L}_0(k) = (t_{0y}, -t_{0x}, 0)$, where $t_{0\nu}$ ($\nu = x, y$) transforms like k_ν . For small $|\mathbf{k}|$, $t_{0\mu} = k_\mu$. In the case of CePt₃Si, CeRhSi₃, and CeIrSi₃, the crystal structures of which have C_{4v} symmetry, the z -component of \mathcal{L}_0 is generally nonzero, but given by $k_x k_y k_z (k_x^2 - k_y^2)$ for small $|\mathbf{k}|$, as elucidated by Samokhin.²¹ However, to highlight the effects of the van-Vleck-like term, we exploit the Rashba type interaction for simplicity. From

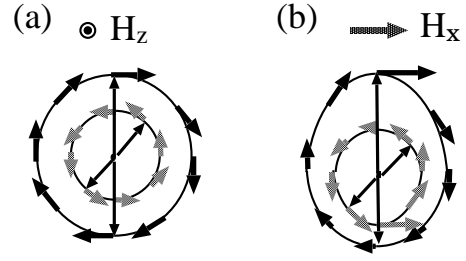


Fig. 4. Effects of the Zeeman magnetic field on the changes of the Fermi surfaces. (a) For magnetic field parallel to z -axis. Arrows on the Fermi surfaces indicate spins. The length of the arrows represents the magnitude of magnetic moments. (b) For in-plane magnetic field.

eq. (21), the single-particle energy in the absence of the Coulomb interaction for $\mathbf{H} = (H_x, 0, H_z)$ is given by

$$\varepsilon_{k\pm} = \varepsilon_k \pm \alpha \sqrt{(t_{0y} - \mu_B H_x)^2 + t_{0x}^2 + \mu_B H_z^2}. \quad (29)$$

It is seen from eq. (29) that magnetic fields parallel to the z -axis merely change the magnitude of the SO splitting of the Fermi surfaces, while magnetic fields parallel to the xy -plane deform the Fermi surfaces into asymmetric shapes, as depicted in Fig.4. These effects indicate that magnetic fields parallel to the z -axis is dominated by the van-Vleck-like susceptibility, while the in-plane magnetic fields induce responses from electron spins corresponding to both the Pauli term and the van-Vleck-like term.

According to the Fermi liquid theory presented in section 2, the exact expression of the spin susceptibility in the superconducting state for the Rashba interaction is obtained as²⁷

$$\chi_{zz}(T) = \mu_B^2 \sum_k \sum_{\tau=\pm} \tau z_{k\tau} \frac{\tanh(\frac{E_{k\tau}}{2T})}{E_{k\tau}} \times \frac{E_{k\tau}^2 + \varepsilon_{k+}^* \varepsilon_{k-}^* + \Delta_{k+} \Delta_{k-}}{E_{k+}^2 - E_{k-}^2} \Lambda^{sz}(E_{k\tau}, \mathbf{k}), \quad (30)$$

for a magnetic field parallel to the z -axis, and

$$\chi_{xx}(T) = \mu_B^2 \sum_{\tau=\pm} \sum_k \frac{z_{k\tau}}{4T \cosh^2(\frac{E_{k\tau}}{2T})} \hat{t}_y \Lambda_\tau^{sx}(E_{k\tau}, \mathbf{k}) + \mu_B^2 \sum_k \sum_{\tau=\pm} \tau z_{k\tau} \frac{\tanh(\frac{E_{k\tau}}{2T})}{E_{k\tau}} \times \frac{E_{k\tau}^2 + \varepsilon_{k+}^* \varepsilon_{k-}^* + \Delta_{k+} \Delta_{k-}}{E_{k+}^2 - E_{k-}^2} \hat{t}_x \Lambda_{+-}^{sx}(E_{k\tau}, \mathbf{k}), \quad (31)$$

for an in-plane magnetic field. Here $E_{k\tau}$ and $\Delta_{k\tau}$ are defined by the equations just below eq. (19). The three-point vertices Λ^{sz} , Λ_{+-}^{sx} , and Λ_τ^{sx} are given by

$$\Lambda^{sz}(p) = 1 - \frac{1}{\mu_B} \frac{\partial \Sigma_0(p)}{\partial H_z}, \quad (32)$$

$$\Lambda_\tau^{sx}(p) = \hat{t}_y (1 - \frac{1}{\mu_B} \frac{\partial \Sigma_x}{\partial H_x}) + \frac{\hat{t}_x}{\mu_B} \frac{\partial \Sigma_y}{\partial H_x} - \frac{\tau}{\mu_B} \frac{\partial \Sigma_0}{\partial H_x}, \quad (33)$$

$$\Lambda_{+-}^{sx}(p) = \hat{t}_x (1 - \frac{1}{\mu_B} \frac{\partial \Sigma_x}{\partial H_x}) - \frac{\hat{t}_y}{\mu_B} \frac{\partial \Sigma_y}{\partial H_x}. \quad (34)$$

Here, $(\hat{t}_x(p), \hat{t}_y(p)) = \hat{\mathbf{t}}(p) = \mathbf{t}(p)/|\mathbf{t}(p)|$, $\mathbf{t}(p) = \mathbf{n} \times \mathcal{L}(p)$ with $\mathbf{n} = (001)$. $\chi_{zz}(T)$ and the second term of $\chi_{xx}(T)$ are the van-Vleck-like susceptibilities. Both the Pauli and van-Vleck-like terms are enhanced by electron correlation effects, because of the three-point vertices.

It is noted that the van-Vleck-like term is quite different from the usual van-Vleck orbital susceptibility, which is caused by symmetric SO interaction, for the following reason. In contrast to the usual van-Vleck term, which is almost independent of temperatures, the van-Vleck-like term due to the parity-breaking SO interaction indeed depends on temperatures, similarly to the Pauli susceptibility, since the magnitude of the parity-breaking SO splitting is much smaller than the Fermi energy for typical heavy fermion systems. According to a simple model calculation based on a two-dimensional tight-binding model on a square lattice carried out by the author, both the Pauli and van-Vleck-like terms exhibit strong temperature dependence, as a result of the energy dependence of the density of states.²⁷ This property implies that it is almost impossible to distinguish between these two contributions experimentally by analyzing the temperature dependence of spin susceptibilities. Thus, we need to be careful about the interpretation of experimental data of spin susceptibilities in the superconducting state, since they always include the van-Vleck-like term which is not strongly affected by superconducting transition when $\Delta \ll E_{\text{SO}}$.

In the case of the Rashba SO interaction, the temperature dependence of spin susceptibilities below T_c was calculated by Gorkov and Rashba, and Frigeri et al. for a model with a spherical Fermi surface.^{5, 15} According to their results, for $\Delta \ll E_{\text{SO}}$, χ_{xx} at zero temperature is one half of the magnitude in the normal state, i.e., $\chi_{xx}(0) = \chi_{xx}(T_c)/2$, owing to the existence of the van-Vleck-like term.

However, experimental observations seem not to be consistent with the theoretical prediction. According to the Knight shift measurements performed by Yogi et al.^{11, 12} for CePt₃Si, both χ_{xx} and χ_{zz} show no significant change even below T_c . To explain the origin of the discrepancy, we note that the magnitude of the ratio $\chi_{xx}(T=0)/\chi_{xx}(T=T_c)$ in the superconducting state crucially depends on the details of the electronic structure and electron correlation effects. For instance, when the density of states has a strong energy dependence, $\chi_{xx}(T=0)/\chi_{xx}(T=T_c)$ may deviate from 1/2. To demonstrate this, we consider a Hubbard-type model on a square lattice with a kinetic energy $\varepsilon_{\mathbf{k}} = -2(\cos k_x + \cos k_y)$, and the Rashba term with $\mathcal{L}_0(\mathbf{k}) = (\sin \frac{k_y}{2}, -\sin \frac{k_x}{2}, 0)$. For this model, at half-filling, we calculate $\chi_{xx}(0)/\chi_{xx}(T_c)$ in the case of $\Delta \ll \alpha|\mathcal{L}|$, handling electron correlation effects by perturbative expansion in terms of U up to the second order and using eq. (31). The results are shown in Fig. 5 As U/W increases, the van-Vleck-like susceptibility is more strongly enhanced by electron correlation than the Pauli term, and the ratio $\chi_{xx}(T=0)/\chi_{xx}(T=T_c)$ approaches 1.0. Although the strength of the electron-electron interaction for which the ratio is nearly equal to 1.0 is consid-

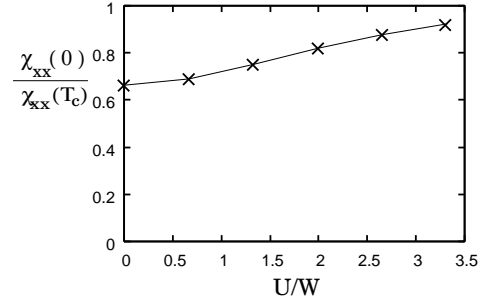


Fig. 5. $\chi_{xx}(T=0)/\chi_{xx}(T=T_c)$ in the superconducting state versus U/W with $\alpha = 1.0$ calculated by second order perturbative expansion with respect to U for the 2D Hubbard-like model.

erably large, the results may be qualitatively valid, and can be improved by including higher order corrections, as long as the system is in the Fermi liquid state. As a matter of fact, CePt₃Si is in the Fermi liquid state with a mass enhancement factor of order ~ 60 , in which the spin susceptibility is also substantially enhanced. Thus, it is possible that, for CePt₃Si, because of strong electron correlation and a particular electronic structure, $\chi_{xx}(T)$ is dominated by the van-Vleck-like term, and thus is almost independent of temperature below T_c , consistent with the NMR measurements.

In the case with cubic symmetry, the uniform spin susceptibilities in the superconducting state are obtained in a similar manner.²⁷ The results are

$$\begin{aligned} \chi_{zz}(T) = & \mu_B^2 \sum_{\tau=\pm} \sum_{\mathbf{k}} \frac{z_{k\tau}}{4T \cosh^2(\frac{E_{k\tau}}{2T})} \Lambda_P^{\text{cub}}(E_{k\tau}, \mathbf{k}) \\ & + \mu_B^2 \sum_{\mathbf{k}} \sum_{\tau=\pm} \tau z_{k\tau} \frac{\tanh(\frac{E_{k\tau}}{2T})}{E_{k\tau}} \\ & \times \frac{E_{k\tau}^2 + \varepsilon_{k+}^* \varepsilon_{k-}^* + \Delta_{k+} \Delta_{k-}}{E_{k+}^2 - E_{k-}^2} \Lambda_V^{\text{cub}}(E_{k\tau}, \mathbf{k}), \end{aligned} \quad (35)$$

where

$$\begin{aligned} \Lambda_P^{\text{cub}}(p) = & \hat{\mathcal{L}}_{0z}^2 \left(1 - \frac{1}{\mu_B} \frac{\partial \Sigma_0(p)}{\partial H_z}\right) \\ & - \frac{\hat{\mathcal{L}}_{0z} \hat{\mathcal{L}}_x}{\mu_B} \frac{\partial \Sigma_x(p)}{\partial H_z} - \frac{\hat{\mathcal{L}}_{0z} \hat{\mathcal{L}}_y}{\mu_B} \frac{\partial \Sigma_y(p)}{\partial H_z}, \end{aligned} \quad (36)$$

$$\begin{aligned} \Lambda_V^{\text{cub}}(p) = & (\hat{\mathcal{L}}_x^2 + \hat{\mathcal{L}}_y^2) \left(1 - \frac{1}{\mu_B} \frac{\partial \Sigma_0(p)}{\partial H_z}\right) \\ & + \frac{\hat{\mathcal{L}}_{0z} \hat{\mathcal{L}}_x}{\mu_B} \frac{\partial \Sigma_x(p)}{\partial H_z} + \frac{\hat{\mathcal{L}}_{0z} \hat{\mathcal{L}}_y}{\mu_B} \frac{\partial \Sigma_y(p)}{\partial H_z}. \end{aligned} \quad (37)$$

Because of the cubic symmetry, $\chi_{xx} = \chi_{yy} = \chi_{zz}$, and χ_{zz} consists of both the Pauli term (the first term on the right-hand side of eq. (35)) and van-Vleck-like term (the second term of (35)). For systems with a spherical Fermi surface, the Pauli term is 1/3 of the total susceptibility. In this case, at zero temperature in the superconducting state, we have $\chi_{zz}(0)/\chi_{zz}(T_c) = 2/3$ for $\Delta \ll E_{\text{SO}}$.

4.2 Pauli limiting field

In this section, we consider the Pauli depairing effect due to the Zeeman magnetic field. This effect in the

case without inversion symmetry was precisely studied by Frigeri et al.¹⁵ The changes of the Fermi surfaces due to the Zeeman magnetic fields depicted in Fig.4 imply that the Pauli depairing effect on Cooper pairs is also unique in noncentrosymmetric superconductors.

We first consider the Rashba case with an asymmetric potential gradient along the z -axis. For magnetic fields parallel to the z -axis, Cooper pairs between electrons with the momenta k and $-k$ are always possible, as shown in Fig.4(a), implying the suppression of the Pauli depairing effect. More precisely, the Pauli limiting field depends on the spin state of Cooper pairs. For spin-triplet pairing states with the \mathbf{d} -vector determined by the Rashba interaction, $\mathbf{d} \propto (t_{0y}, -t_{0x}, 0)$, the pairing state with $S_z = \pm 1$ for the spin quantization axis parallel to the z -axis is realized. Magnetic fields parallel to the z -axis do not give rise to the Pauli depairing effect on this state. On the other hand, for spin singlet states, the Pauli limiting field exists. However, it is strongly enhanced by the parity-breaking SO interaction. To argue the Pauli depairing effect on the singlet state, we consider a simple case without electron correlation, and assume the attractive interaction $-Vw_k w_{-k}$ for a singlet channel, where w_k is a structure factor for the orbital degrees of freedom. We also assume that E_{SO}/E_F is sufficiently small, and that the admixture of triplet states is negligible. Then, the gap equation for $H_z \neq 0$ is given by

$$\frac{1}{V} = \sum_k \sum_{\tau=\pm 1} \frac{\alpha^2 |t_0|^2 w_k^2}{\alpha^2 |t_0|^2 + \mu_B^2 H_z^2} \frac{\tanh \frac{E_{k\tau}}{2T}}{4E_{k\tau}} + \sum_k \sum_{\tau=\pm 1} \frac{w_k^2 \mu_B^2 H_z^2}{\alpha^2 |t_0|^2 + \mu_B^2 H_z^2} \frac{\zeta_{k\tau} \tanh \frac{E_{k\tau}}{2T}}{4E_{k\tau}}, \quad (38)$$

where

$$\zeta_{k\tau} = 1 + \tau \frac{\alpha^2 |t_0|^2 + \mu_B^2 H_z^2}{\sqrt{\varepsilon_k^2 (\alpha^2 |t_0|^2 + \mu_B^2 H_z^2) + \mu_B^2 H_z^2 \Delta_k^2}}, \quad (39)$$

$$E_{k\tau} = \pm [\varepsilon_k^2 + \alpha^2 |t_0|^2 + \mu_B^2 H_z^2 + \Delta_k^2 + 2\tau \sqrt{\alpha^2 |t_0|^2 + \mu_B^2 H_z^2} \sqrt{\varepsilon_k^2 + \Delta_k^2 (\xi_+^2 - \xi_-^2)}]^{1/2} \quad (40)$$

and $|t_0|^2 = t_{0x}^2 + t_{0y}^2$, $\Delta_k = \Delta_0 w_k$. It is evident that for $\mu_B H_z \ll \alpha |t_0|$, the first term on the right-hand side of eq. (38) dominates over the second term, and thus the Pauli depairing effect is negligible. For general values of H_z , the transition temperature T_c is determined by using the linearized gap equation. It is noted that the first term on the right-hand side of (38) in the linearized approximation yields a $\log T$ singularity at low temperatures for any finite values of H_z which satisfies $\mu_B H_z < E_F$, while the second term exhibits no logarithmic singularity. As a result, the finite transition temperature T_c always exists for any finite magnetic field $H_z < E_F$. This implies that the Pauli limiting field is infinitely large for sufficiently low temperatures. According to precise numerical calculations performed by Frigeri et al., the Pauli limiting field determined by the linearized gap equation obeys a concave curve on the H - T plane at sufficiently low temperatures.¹⁵ It is noteworthy that the recent experiments on CeRhSi₃ support the existence of the large upper critical fields at low temperatures exceeding a conventional

Pauli limit, and exhibiting a concave behavior as a function of T .⁴² In these experiments, although the concave behavior is observed even near T_c , it is expected that the inclusion of the strong-coupling effect enlarges the temperature region where the concave behavior appears up to higher temperatures close to T_c .

Also, the above results are easily obtained from a simple thermodynamic argument. Let $\chi_{zz,N}$ and $\chi_{zz,S}$ be the spin susceptibilities in the normal and superconducting states, respectively, for a magnetic field parallel to the z -axis. Then, the Pauli limiting field H_P at zero temperature is determined by equating the ground state energy in the normal state to that in the superconducting state

$$\frac{\chi_{zz,N} H_P^2}{2} = \frac{\chi_{zz,S} H_P^2}{2} + \frac{N(0) \Delta_0^2}{2}, \quad (41)$$

which leads to $H_P = \Delta_0 \sqrt{N(0)/(\chi_{zz,N} - \chi_{zz,S})}$, where $N(0)$ is the average density of states of the SO splitted two bands. We see from eq.(30) that when $\Delta_0 \ll E_{\text{SO}}$, $\chi_{zz,N} - \chi_{zz,S} \approx \chi_{zz,N} (\Delta_0/E_{\text{SO}})^2 \ll \chi_{zz,N}$ holds, leading to a large H_P enhanced by the factor E_{SO}/Δ_0 . More precisely, the free energy difference between the superconducting state and the normal state at any finite temperatures is calculated from $\Omega_s - \Omega_n = \int_0^{\Delta_0} (dV^{-1}/d\Delta) \Delta^2 d\Delta$. By carrying out numerical calculations, one can confirm that when the gap equation (38) gives a nonzero value of Δ_0 , $\Omega_s - \Omega_n < 0$ holds at least for $\Delta_0 < E_{\text{SO}}$, and thus the superconducting state is the absolute minimum of the free energy; i.e. H_P determined by using the linearized gap equation coincides with that obtained from the thermodynamic consideration.

For magnetic fields parallel to the xy -plane, the Fermi surfaces are deformed into asymmetric shapes as shown in Fig. 4(b), which gives rise to the Pauli depairing effect for both spin singlet and spin triplet states. The Pauli depairing effect stems from the Pauli term of the spin susceptibility χ_{xx} , i.e., the first term of eq. (31). When $\Delta_0 \ll E_{\text{SO}}$, and $\chi_{xx,N}^{\text{van Vleck}} - \chi_{xx,S}^{\text{van Vleck}} \approx \chi_{xx,N}^{\text{van Vleck}} (\Delta_0/E_{\text{SO}})^2 \ll \chi_{xx,N}^{\text{van Vleck}}$, $\chi_{xx,N}^{\text{Pauli}}$ holds, the Pauli limiting field is $H_P \approx \Delta_0 \sqrt{N(0)/(\chi_{xx,N}^{\text{Pauli}} - \chi_{xx,S}^{\text{Pauli}})}$.

In the case with a spherical Fermi surface but without electron correlation, $\chi_{xx,N}^{\text{Pauli}}$ is one half of the total spin susceptibility. Thus, at zero temperature where $\chi_{xx,S}^{\text{Pauli}} = 0$, H_P is enhanced by a factor of $\sqrt{2}$, compared to the case with inversion symmetry in which the Pauli limiting field is $H_P^{\text{inv.sym.}} = \Delta_0/\sqrt{2}$. However, the real situation is more complicated. According to a more precise analysis done by Kaur et al. and Samokhin, the asymmetric deformation of the Fermi surface due to in-plane magnetic fields may stabilize Cooper pairs with a center of mass momentum, leading to the Fulde-Ferrel state.^{16,19} We would like to discuss this point in section 4.6.

In the case with cubic symmetry, the spin susceptibility consists of both the Pauli and van Vleck-like terms, and an argument similar to that for the Rashba model with in-plane magnetic fields is applicable. When $\Delta_0 \ll E_{\text{SO}}$ holds, the Pauli limiting field is given by $H_P \approx \Delta_0 \sqrt{N(0)/(\chi_{zz,N}^{\text{Pauli}} - \chi_{zz,S}^{\text{Pauli}})}$. Here, $\chi_{zz,S}^{\text{Pauli}}$ is the first term on the right-hand side of eq. (35) in the su-

perconducting (normal) state. In the case with a spherical Fermi surface without electron correlation, at zero temperature, $\chi_{zz,N}^{\text{Pauli}}$ is 1/3 of the total susceptibility, as claimed in the previous section, and thus H_P is enhanced by a factor of $\sqrt{3}$ compared with that in the case with inversion symmetry.

4.3 Nuclear relaxation rate $1/T_1$

One of powerful experimental probes for superconducting states is the NMR measurement of the nuclear relaxation rate $1/T_1$. For conventional superconductors with the s -wave symmetry, $1/T_1$ exhibit a coherence peak just below T_c , and an exponential decay at low temperatures. For unconventional superconductors with an inversion center such as High- T_c cuprates, and many heavy fermion systems, there is no coherence peak, because of the absence of the coherence factor and the suppressed singularity of the density of states, and also a power law decay at low temperatures appears. In the case without inversion symmetry, a quite different behavior is theoretically expected, as pointed out by the present author and Hayashi et al.^{22,23}

For simplicity, we neglect electron correlation effects, which may not change the following argument drastically. Then, the nuclear relaxation rate is given by

$$\begin{aligned} \frac{1}{T_1 T} &\propto \\ \lim_{\omega \rightarrow 0} \frac{1}{\omega} \text{Im} &\left[T \sum_{\varepsilon_m} \sum_{k, k'} \left\{ \text{Tr} \left[\frac{\sigma^+}{2} \hat{G}(\varepsilon_m + \omega_n, k) \frac{\sigma^-}{2} \hat{G}(\varepsilon_m, k') \right] \right. \right. \\ &\left. \left. - \text{Tr} \left[\frac{\sigma^+}{2} \hat{F}(\varepsilon_m + \omega_n, k) \frac{\sigma^-}{2} \hat{F}(\varepsilon_m, k') \right] \right\} \right]_{i\omega_n \rightarrow \omega + i\delta} \\ &= \int \frac{d\varepsilon}{2\pi} \frac{1}{2T \cosh^2 \frac{\varepsilon}{2T}} \{ [N_n(\varepsilon)]^2 + [N_a(\varepsilon)]^2 \}, \end{aligned} \quad (42)$$

with $N_n(\varepsilon)$ and $N_a(\varepsilon)$ defined by the retarded Green's functions as

$$N_n(\varepsilon) = - \sum_k \sum_{\tau=\pm} \text{Im} G_{\tau}^R(\varepsilon, k), \quad (43)$$

$$N_a(\varepsilon) = - \sum_k \sum_{\tau=\pm} \text{Im} F_{\tau}^R(\varepsilon, k). \quad (44)$$

$N_a(\varepsilon)$ gives the coherence factor, which enhances the coherence peak of $1/T_1 T$. For unconventional pairing states with the angular momentum $\ell \geq 2$, the coherence factor vanishes. A remarkable feature of $1/T_1 T$ for non-centrosymmetric superconductors appears in the case of the p -wave state. In contrast to the case with inversion symmetry in which the coherence factor vanishes for the p -wave state, the absence of inversion symmetry gives rise to nonzero coherence factor N_a for the p -wave state. This is easily understood as follows. In the case of the pure p -wave state, the superconducting gap is given by $\Delta(\hat{k}) = \Delta_t \mathcal{L}(k) \cdot \sigma i \sigma_y$ where $\mathcal{L}(k)$ has the p -wave symmetry. An important point is that the factor $\mathcal{L}(k)$ appears in eq. (44) only in the form $|\mathcal{L}(k)|$. (see eqs.(20) and (19)) Thus, when the density of states for the (+)-band is different from that for the (-)-band, $N_a(\varepsilon)$ is nonzero. This result implies that the coherence peak of $1/T_1 T$ just

below T_c is markedly enhanced in the case of the p -wave pairing dominated state. The implication of this result for CePt₃Si will be discussed in section 5.

4.4 Magnetoelectric effect in the normal state

The existence of the asymmetric SO interaction $\alpha \mathcal{L}_0(k) \cdot \sigma$ yields a nontrivial coupling between charge and spin degrees of freedom, giving rise to interesting electromagnetic properties. One example is the existence of magnetoelectric effects. Magnetoelectric effects in a normal metal were discussed by Levitov et al. many years ago within one-body approximation.^{43,44}

In the case of the Rashba SO interaction with $\mathcal{L}_0(k) = (t_{0y}(k), -t_{0x}(k), 0)$, the magnetization along the x -direction is generated by an electric field applied in the y -direction as

$$M_x = \Upsilon_{xy} E_y, \quad (45)$$

and conversely an AC-magnetic field gives rise to a charge current flow expressed as

$$J_x = -2\Upsilon_{xy} \frac{\partial B_y}{\partial t}. \quad (46)$$

The physical origin of these effects is easily understood as follows. As shown in Fig. 6 (a), when charge current flows along the y -axis, the Fermi surface is deformed, and because of the Rashba SO interaction, the distribution of spins changes, yielding the bulk magnetization along the x -axis. Conversely, an applied magnetic field in the x -direction changes the distribution of spins, which also deforms the Fermi surface asymmetrically, leading to a charge current in the y -direction.

In the case of heavy fermion systems, the magnetoelectric effect coefficient Υ_{xy} is significantly affected by strong electron correlation. According to the analysis based on the Fermi liquid theory, we obtain a simple relation among Υ_{xy} , the specific heat coefficient γ , and the resistivity ρ :²⁷

$$\Upsilon_{xy} \sim \frac{\mu_B}{ev_F^* \rho} \cdot \frac{\alpha k_F}{E_F} \propto \frac{\gamma}{\rho}. \quad (47)$$

In general, for heavy fermion systems, the resistivity is given by $\rho \sim \rho_0 + \text{const.} \gamma^2 T^2$, with ρ_0 a residual resistivity. Thus, at sufficiently low temperatures, Υ_{xy} is enhanced by the factor γ .

We now estimate the order of the magnitude of these effects. We assume that the Fermi velocity is $v_F^* \sim 10^5$ cm/s, which corresponds to a mass enhancement of order ~ 100 , and the SO splitting is sufficiently large, e.g., $\alpha k_F / E_F \sim 0.1$. To consider the magnetization induced by an electric field, we assume that the charge current density is $J \sim 1$ A/cm². Then, the induced magnetization is estimated as, $M = \Upsilon_{xy} E_y \approx \mu_B (\alpha k_F / E_F) (J / ev_F^*) \sim 1$ Gauss, which is experimentally measurable. To evaluate the charge current induced by AC magnetic fields we assume that an AC magnetic field $B = B_0 \cos(\omega t)$ with $B_0 \sim 100$ Gauss, and $\omega \sim 100$ kHz is applied, and that the normal resistivity is $\rho \sim 10 \mu\Omega \cdot \text{cm}$. Then we obtain the charge current, $J = -2\Upsilon_{xy} (dB/dt) \approx \mu_B (\alpha k_F / E_F) (dB/dt) / (ev_F^* \rho) \sim 1$ mA/cm². This magnitude is also experimentally accessible. However, in this case, it is necessary to distinguish

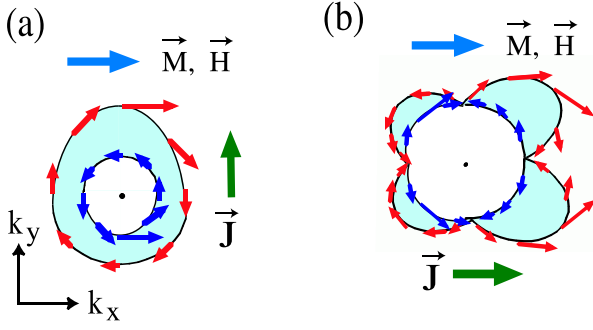


Fig. 6. (Color online) Changes of the Fermi surfaces and the spin configuration due to applied magnetic field (or net current flow). (a) For the Rashba interaction, current flow along the y -axis gives rise to magnetization along the x -axis. Conversely, an applied magnetic field along the x -axis yields current flow along the y -axis. (b) For the Dresselhaus interaction, the current flow is parallel to the applied magnetic field (or induced magnetization). A sectional view for $k_z = 0$ is shown.

between the magnetoelectric effect and the usual eddy current induced by the time-dependent magnetic field. To avoid the eddy current, leads attached to the sample must be aligned exactly parallel to the magnetic field.

A similar effect is also possible in cubic systems without inversion symmetry. In this case, the charge current (or applied electric fields) is parallel to magnetic fields (or magnetization) as shown in Fig. 6 (b), i.e., $\mathbf{J} = -2\Upsilon(d\mathbf{B}/dt)$. The coefficient Υ is approximately given by eq. (47).

4.5 Magnetoelectric effect in the superconducting state

Magnetoelectric effects in the superconducting state analogous to those in the normal state are possible. These phenomena were theoretically predicted by Edelstein, and extensively discussed by Yip and the present author.^{1, 2, 6, 20, 22, 27} In the absence of inversion symmetry, supercurrent can be induced by the Zeeman magnetic field, which may be called “paramagnetic supercurrent”.^{1, 6} Conversely, bulk magnetization is raised by supercurrent flow.² The physical origin of these effects is also the asymmetric deformation of the Fermi surface due to an applied magnetic field as in the case of the normal state. However, in contrast to the analogous effects in the normal state, the magnetoelectric effects in the superconducting state are dissipationless. As a result, to detect the paramagnetic supercurrent flow experimentally, one needs to prepare a system in which the dissipationless bulk current is possible. One example of such a system may be realized by attaching leads made of superconductors to the sample.⁴⁵

To explain the above-mentioned effects in more detail, we first use the Ginzburg-Landau (GL) theory, and later, we will present microscopic analysis. The GL free energy for superconductors without inversion symmetry was derived by Edelstein, Samokhin, and Kaur et al.,^{3, 16, 19} which reads,

$$F_s - F_n = a|\Psi|^2 + \frac{\beta}{2}|\Psi|^4 + \frac{1}{2m_\mu}|D_\mu\Psi|^2$$

$$+ \frac{\mathcal{K}_{\mu\nu}}{2en_s} B_\mu (\Psi(D_\nu\Psi)^* + \Psi^* D_\nu\Psi) + \frac{B^2}{8\pi} - \frac{\chi_{\mu\mu} B_\mu^2}{2}, \quad (48)$$

where $a = a_0(T - T_{c0})$, $D_\mu = -\hbar\nabla_\mu - 2eA_\mu/c$, A_μ is a vector potential, $\mathbf{B} = \nabla \times \mathbf{A}$, \mathbf{M} is the magnetization density, and n_s is the superfluid density. The fourth term of eq. (48) with the coefficient $\mathcal{K}_{\mu\nu}$ stems from the parity-breaking SO interaction, and is the origin of magnetoelectric effects. Differentiating the free energy with respect to \mathbf{A} and \mathbf{B} , we obtain the following relations for the supercurrent density \mathbf{J}^s and the magnetization density \mathbf{M} .

$$\mathbf{J}_\mu^s = \mathbf{J}_\mu^{\text{dia}} + \mathcal{K}_{\nu\mu} B_\nu, \quad (49)$$

$$\mathbf{M}_\mu = \mathcal{K}_{\mu\nu} \Lambda \mathbf{J}_\nu^{\text{dia}} + \mathbf{M}_\mu^{\text{Zee}}. \quad (50)$$

Here, $\mathbf{J}_\mu^{\text{dia}}$ is the conventional diamagnetic supercurrent given by $\mathbf{J}_\mu^{\text{dia}} = (\hbar\nabla_\mu\phi - 2eA_\mu/c)/(2e\Lambda)$. ϕ is the phase of the order parameter Ψ . $\Lambda^{-1} = 2e^2|\Psi|^2/m$. $\mathbf{M}_\mu^{\text{Zee}}$ is a magnetization due to the conventional Zeeman effect. Also, we have put $|\Psi|^2 = n_s$. The second term on the right-hand side of eq. (49) is the paramagnetic supercurrent, and the first term on the right-hand side of eq. (50) is the magnetization induced by supercurrent flow. In the case of the Rashba interaction, $\mathcal{K}_{\mu\nu}$ is nonzero only for $(\mu, \nu) = (x, y)$ or (y, x) . In the case of cubic systems, $\mathcal{K}_{\mu, \nu} = \mathcal{K}\delta_{\mu\nu}$.

As was pointed out by Yip, in the case of the Rashba interaction, the paramagnetic supercurrent is partially canceled with the magnetization current $\mathbf{J}^M = c\nabla \times \mathbf{M}$.²⁰ To observe this, using eqs. (49), (50), and the relation $\nabla \times \mathbf{J}^{\text{dia}} = -\mathbf{B}/c\Lambda$, we write down the total current,

$$\mathbf{J}_s + \mathbf{J}_M = \mathbf{J}^{\text{dia}} + c\nabla \times \mathbf{M}^{\text{Zee}} + c\mathcal{K}\Lambda(-\partial_x J_z^{\text{dia}}, \partial_y J_z^{\text{dia}}, \partial_x J_x^{\text{dia}} + \partial_y J_y^{\text{dia}}). \quad (51)$$

The last term on the right-hand side of eq. (51) is the paramagnetic supercurrent. In the complete Meissner state and in the thermodynamic limit, this term vanishes, and thus there is no paramagnetic supercurrent. Yip pointed out that because of this cancellation, the penetration depth is symmetric under the transformation $z \rightarrow -z$.²⁰ However, in finite systems, or in the mixed state, the last term of eq. (51) gives nonzero contributions to the magnetoelectric effect.

In the case of cubic systems, the cancellation between the paramagnetic supercurrent and the magnetization current is perfect. This is easily seen as follows. Since in cubic systems $\mathcal{K}_{\mu\nu} = \mathcal{K}\delta_{\mu\nu}$, we obtain $\mathbf{J}^s = \mathbf{J}^{\text{dia}} + \mathcal{K}\mathbf{B}$, $\mathbf{M} = \mathcal{K}\Lambda\mathbf{J}^{\text{dia}} + \mathbf{M}^{\text{Zee}}$, and $\mathbf{J}^M = c\nabla \times \mathbf{M} = -\mathcal{K}\mathbf{B} + c\nabla \times \mathbf{M}^{\text{Zee}}$, and as a result, the paramagnetic current $\mathcal{K}\mathbf{B}$ cancels exactly in the total current $\mathbf{J}^s + \mathbf{J}^M$. There is no paramagnetic supercurrent in this case.

The magnetoelectric effect coefficient $\mathcal{K}_{\mu\nu}$ can be obtained from microscopic calculations as in the case of the normal state. According to the Fermi liquid theory explained in section 2, the formula of \mathcal{K}_{yx} , which includes

electron correlation effects exactly, is given by^{22,27}

$$\begin{aligned} \frac{\mathcal{K}_{yx}}{e\mu_B} = & \sum_k \sum_{\tau=\pm 1} \tau v_{0y\tau} \frac{z_{k\tau} \Delta_{k\tau}^2}{E_{k\tau}^2} \left[\frac{\text{ch}^{-2} \frac{E_{k\tau}}{2T}}{2T} - \frac{\text{th} \frac{E_{k\tau}}{2T}}{E_{k\tau}} \right] \Lambda_{\tau}^{sx}(E_{k\tau}, \mathbf{k}) \\ & + 2\alpha \sum_k \frac{\Delta_{k+} \Delta_{k-}}{E_{k+}^2 - E_{k-}^2} \left[z_{k-} \frac{\text{th} \frac{E_{k+}}{2T}}{E_{k+}} - z_{k+} \frac{\text{th} \frac{E_{k-}}{2T}}{E_{k-}} \right] \\ & \times \hat{t}_x \Lambda_{+-}^{sx}(E_{k\tau}, \mathbf{k}), \end{aligned}$$

where $v_{0y\tau} = \partial(\varepsilon_k + \tau\alpha|t_0|)/\partial k_y$. In the case with a spherical Fermi surface, up to the first order in $\alpha k_F/E_F$, the magnetoelectric coefficient is simplified as

$$\mathcal{K}_{\mu\nu} = \frac{e\mu_B n_s \alpha}{8\pi^3 z E_F}, \quad (53)$$

where n_s is the superfluid density. Note that \mathcal{K}_{yx} is amplified by the mass enhancement factor $1/z_{k\tau}$, when the Wilson ratio is nearly equal to 2, as realized in typical heavy fermion systems. This feature is in contrast to the electron correlation effect on the diamagnetic supercurrent which is suppressed by the factor $z_{k\tau}$. As a result, the magnetoelectric effect in the superconducting state is more strongly enhanced in heavy fermion systems with large effective mass than in weakly correlated metals.

We now discuss the feasibility of experimental observations of these effects. Assuming that $\alpha k_F/E_F \sim 0.1$, the electron density $n \sim 10^{22} \text{ cm}^{-3}$, the mass enhancement factor $1/z \sim 100$, and $v_s/v_F^* \sim \Delta/E_F \sim 0.01$, we estimate the magnitude of the bulk magnetization induced by the supercurrent as $M = \mathcal{K} \Lambda J^{\text{dia}} \approx \mu_B n (\alpha k_F/E_F) (v_s/v_F^*) / (8\pi^3 z) \sim 0.1 \text{ Gauss}$. The experimental detection of this internal field may be possible. Under the above conditions, the magnitude of the paramagnetic supercurrent is also accessible by conventional experimental measurements. It should be emphasized again that to detect paramagnetic supercurrent, one needs to prepare a circuit in which bulk current flow without dissipation is possible. Also, in the mixed state, vortices should be pinned by impurities to suppress dissipation due to the flux flow, which may be induced by supercurrent, as demonstrated by Oka et al.²⁶

4.6 Helical vortex state (Fulde-Ferrel state)

In the previous section, we have seen that the asymmetric deformation of the Fermi surface due to an applied magnetic field may give rise to the paramagnetic supercurrent, if the dissipationless bulk current flow is permitted. Conversely, when bulk current flow is forbidden, as in the case of an isolated system, the asymmetric deformation of the Fermi surface stabilizes an inhomogeneous superconducting state with a finite phase gradient. This possibility was first pointed out by Kaur et al. and Samokhin.^{16,19} They argued that in the Rashba case, an in-plane magnetic field applied to an isolated system gives rise to a Fulde-Ferrel-like state, in which Cooper pairs have a center of mass momentum and the phase of the order parameter is spatially modulated.^{16,19} Kaur et al. called this novel phase the helical vortex state. Following their analysis, we would like to consider this phase

on the basis of the GL free energy (48). From the derivative of eq. (48) with respect to Ψ , one finds that a stable solution is given by $\Psi(R) = \Psi_0(R) e^{-i\mathbf{q} \cdot \mathbf{R}}$ with¹⁹

$$q_\mu = -\frac{2m\mathcal{K}_{\nu\mu}}{\hbar n_s} B_\nu. \quad (54)$$

Here $\Psi_0(R)$ is the solution of the GL free energy without the parity-breaking term (the fourth term of eq.(48)). This corresponds to a Fulde-Ferrel state with a spatial modulation of the order parameter phase. It is noted that the period of the modulation $1/q_\mu$ decreases as $\sim z_{k\tau}^2$, as the effective electron mass $1/z_{k\tau}$ increases. When $1/q_\mu$ is smaller than the spacing between vortices, the helical vortex phase governs the upper critical field. The critical temperature at finite \mathbf{B} in this phase is derived by using the standard method,^{16,19}

$$T_c(\mathbf{B}) = T_c(0) - \frac{\pi B}{\Phi_0 m a_0} + \frac{\mathcal{K}_{\mu\nu}^2 m}{8a_0 e^2 n_s^2} B^2. \quad (55)$$

Thus, the transition temperature (or the upper critical field) is increased by the inversion-symmetry breaking term of the free energy (48). We would like to emphasize that the increase in $T_c(\mathbf{B})$ is drastically amplified by electron correlation effects, since the last term of the right-hand side of (55) is enhanced by the factor $1/z_{k\tau}^3$, while the second term corresponding to the conventional orbital depairing effect is suppressed by the factor $z_{k\tau}$. Therefore, the realization of the helical vortex state is feasible in heavy fermion systems. To estimate the order of the magnitude of this effect, let us assume that, as in the case of CePt₃Si, the ratio of the SO splitting to the Fermi energy $\alpha k_F/E_F$ is ~ 0.1 , the mass enhancement factor $1/z_{k\tau}$ is of order ~ 100 , the Fermi velocity is $v_F^* \sim 10^5 \text{ cm/s}$, the upper critical field is $H_{c2} \sim 4 \text{ T}$, and the applied magnetic field B is close to H_{c2} . Then, the period of the spatial modulation is estimated as $1/q \sim \mu_B B / (16\pi^3 v_F^* z) \cdot (\alpha k_F/E_F) \sim 10^{-6} \text{ cm}$, which is compatible with the inter-vortex distance. In this situation, the increase in T_c due to the Helical vortex phase is almost on the same order as the decrease due to the orbital depairing effect, and plays a crucial role in the vicinity of the upper critical field.

4.7 Anomalous Hall effect

In general, the SO interaction can yield the anomalous Hall effect, as clarified by Karplus-Luttinger many years ago.⁴⁶ The anomalous Hall effect stems from the anomalous velocity which is caused by the SO interaction. In the case of the Rashba SO interaction, this mechanism can be schematically illustrated as shown in Fig.7. When an electric field applied along the y -axis induces current flow along this direction, the Fermi surfaces are deformed asymmetrically, and thus the distribution of spins, which is constrained by the Rashba SO interaction, is changed as shown in Fig.7(a). Then, a magnetic field applied along the z -axis gives rise to a torque which rotates spins around the z -axis as depicted in Fig.7(b). Since the Rashba SO interaction forces the Fermi momentum to be perpendicular to spins, the asymmetric Fermi surfaces are rotated on the xy -plane. As a consequence, the net current along the x -axis occurs as shown

in Fig.7(c). In the case of the Rashba interaction, the anomalous velocity $\mathbf{v}_A = \alpha \nabla \mathbf{t}_0(\mathbf{k}) \cdot (\mathbf{n} \times \boldsymbol{\sigma})$ is perpendicular to the z -axis. Thus, the anomalous Hall effect is possible only for magnetic fields along the z -axis. According to the analysis based on the Fermi liquid theory, the anomalous Hall conductivity in the normal state is expressed as²⁷

$$\frac{\text{Re } \sigma_{xy}^{\text{AHE}}}{H_z} = e^2 \mu_B \sum_{\tau=\pm} \sum_{\mathbf{k}} \frac{-\tau f(\varepsilon_{k\tau}^*) \Lambda^{sz}(\varepsilon_{k\tau}^*, \mathbf{k})}{2\alpha |\text{Re } \mathbf{t}(\varepsilon_{k\tau}^*, \mathbf{k})|^3} \times (\partial_{k_x} t_{x\tau} \partial_{k_y} t_{0y} - \partial_{k_x} t_{y\tau} \partial_{k_y} t_{0x}). \quad (56)$$

This quantity is enhanced by the factor Λ^{sz} , which is equal to the enhancement factor of the van-Vleck-like spin susceptibility (30). For heavy fermion systems, this factor is of the same order as the mass enhancement factor $1/z_{k\tau} \approx 100 \sim 1000$, and thus, the anomalous Hall effect is significantly large. For instance, let us assume the resistivity $\rho \sim 10 \mu\Omega \cdot \text{cm}$, the mass enhancement factor $1/z_{k\tau} \sim 100$, the Fermi velocity $v_F^* \sim 10^5 \text{ cm/s}$, and the carrier density $n \sim 10^{22} \text{ cm}^{-3}$. Then, the ratio of $\sigma_{xy}^{\text{AHE}} \sim e^2 \mu_B B / (\hbar^2 v_F^* z)$ to the normal Hall conductivity σ_{xy}^{NHE} is estimated as $\sigma_{xy}^{\text{AHE}} / \sigma_{xy}^{\text{NHE}} \sim 40$. The anomalous Hall effect dominates over the normal Hall effect.

An analogous effect of heat current is also possible. The anomalous Hall conductivity for heat current is expressed as²⁷

$$\kappa_{xy}^{\text{AHE}} = \frac{1}{T} (L_{xy}^{(2)} - \sum_{\mu\nu} L_{x\mu}^{(1)} L_{\mu\nu}^{(0)-1} L_{\nu y}^{(1)}), \quad (57)$$

where $L_{\mu\nu}^{(0)}$ is equal to the conductivity tensor $\sigma_{\mu\nu}$ and

$$\frac{L_{xy}^{(m)\text{AHE}}}{H_z} = e^{2-m} \mu_B \sum_{\tau=\pm} \sum_{\mathbf{k}} (-\tau) (\varepsilon_{k\tau}^*)^m f(\varepsilon_{k\tau}^*) \times \frac{\Lambda^{sz}(\varepsilon_{k\tau}^*, \mathbf{k})}{2\alpha |\text{Re } \mathbf{t}(\varepsilon_{k\tau}^*, \mathbf{k})|^3} (\partial_{k_x} t_{x\tau} \partial_{k_y} t_{0y} - \partial_{k_x} t_{y\tau} \partial_{k_y} t_{0x}), \quad (58)$$

with $m = 1, 2$.

Note that in eqs. (56) and (58), electrons away from the Fermi surface give dominant contributions to the anomalous Hall conductivity. This feature is in accordance with the fact that the magnetic response against the magnetic field along the z -axis is governed by the van-Vleck-like term. This observation leads us to an interesting implication for the superconducting state. In the superconducting state, the Hall effect for heat current is possible at finite temperatures, and when the superconducting gap is much smaller than the size of the SO splitting, the thermal anomalous Hall conductivity is not affected by the superconducting transition. Furthermore, even in the limit of zero temperature, $\kappa_{xy}^{\text{AHE}} / (TH_z)$ is nonzero, and behaves as in the normal state, even though the quasiparticle density is vanishingly small. The experimental detection of this effect is an intriguing future issue.

5. Pairing State Realized in CePt₃Si

In recent years, several heavy fermion superconductors without inversion symmetry have been discovered. In particular, extensive experimental studies on the superconducting state in CePt₃Si have revealed several important aspects of this system. In this section, we would

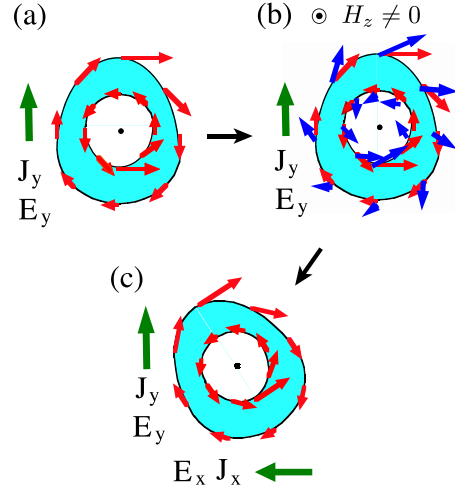


Fig. 7. (Color online) Schematic explanation for anomalous Hall effect. (a) An applied electric field along the y -axis changes the distribution of spin. (b) Torque produced by magnetic field along the z -axis rotates spins. (c) Because of the Rashba SO interaction, the Fermi surface is deformed, leading to a transverse current along the x -axis.

like to discuss about possible pairing states realized in CePt₃Si, comparing the recent experimental data with the theoretical understanding of noncentrosymmetric superconductors.

As mentioned in the previous sections, the \mathbf{d} -vector of the spin triplet component is determined by the parity-breaking SO interaction. In the case of CePt₃Si which has the crystal structure with the C_{4v} symmetry, the possible form of the parity-breaking SO interaction $\alpha \mathbf{L}_0(\mathbf{k}) \cdot \boldsymbol{\sigma}$ was clarified by Samokhin from a general group theoretical argument.²¹ According to his analysis, there are three constraint conditions that determine the form of $\mathbf{L}_0(\mathbf{k})$: (i) $\mathbf{L}_0(-\mathbf{k}) = -\mathbf{L}_0(\mathbf{k})$. (ii) $\mathbf{L}_0(\mathbf{k})$ satisfies the symmetry of the point group. (iii) $\mathbf{L}_0(\mathbf{k})$ is a pseudovector which changes its sign under the transformation $(k_x, k_y, k_z) \rightarrow (k_y, k_x, k_z)$, $(x, y, z) \rightarrow (y, x, z)$, since it is a quantum mechanical average of the operator $\nabla V \times \mathbf{k}$.^{21,48} Then, the general form of $\mathbf{L}_0(\mathbf{k})$ for C_{4v} symmetry is given by $\mathbf{L}_0(\mathbf{k}) = (k_y, -k_x, c_0 k_x k_y k_z (k_x^2 - k_y^2))$.²¹ For periodic systems, k_μ and k_μ^2 are, respectively, replaced by $\sin k_\mu$ and $\cos k_\mu$. The coefficient c_0 of the z -component depends on microscopic detail of the system. The case of $c_0 = 0$ corresponds to the Rashba interaction. In this case, the \mathbf{d} -vector proportional to $(k_y, -k_x, 0)$ gives the highest T_c , as clarified by Frigeri et al.¹⁵ In the case of $c_0 \neq 0$, the situation is more complicated, because the magnitude of the pairing interaction for the channel corresponding to the basis function $k_x k_y k_z (k_x^2 - k_y^2)$ (the A_2 representation of C_{4v}) is generally different from that for the p -wave channel corresponding to the E representation of C_{4v} , and thus $\mathbf{d} \neq \Delta_t(\mathbf{k}) \mathbf{L}_0(\mathbf{k})$, leading to depairing effects, as mentioned in section 2. The pairing state in this case is determined by the competition between the strength of the pairing interaction and the pair-breaking effect due to the SO interaction. In the following, we assume that c_0 is sufficiently small for simplicity, and that the Rashba type interaction is applicable to this system, i.e.,

$\mathbf{d} \propto (k_y, -k_x, 0)$.

One remarkable experimental observation for CePt₃Si which is relevant to the pairing state was obtained from the NMR measurements of $1/T_1$ by Yogi et al.^{11,12} According to their data, $1/T_1$ exhibit a small coherence peak just below T_c , indicating a fully gapped state. Another important experimental observation was obtained from the thermal transport measurements by Izawa et al.¹³ They found that at low temperatures the thermal conductivity exhibits the Volovik effect, indicating the existence of line nodes of the superconducting gap. Also, the results of the penetration depth measurement,¹⁴ and the specific heat measurement⁴⁷ support the existence of the line nodes at sufficiently low temperatures. Thus, for the clarification of the pairing state, it is crucial to reconcile the existence of the coherence peak of $1/T_1$ with the line node of the superconducting gap. In general, the coherence peak of $1/T_1$ is due to the coherence factor and the singularity of the density of states at the gap edge. Even for unconventional superconductors with line nodes, the singularity of the density of states exists, and may give rise to a small coherence peak. However, in strongly correlated electron systems, because of the large quasiparticle damping, the singularity is smeared out, and as a result, no coherence peak is observed for all unconventional superconductors in heavy fermion systems except CePt₃Si. In CePt₃Si, the quasiparticle damping is quite large as indicated by the resistivity data in the normal state. Thus, the existence of a coherence peak cannot be explained by the singularity of the density of states. Also, it is very unlikely that the s -wave pairing is realized in such heavy fermion systems with the large onsite repulsion. Therefore, we need to give some specific reason for this remarkable feature. As argued in section 4.3, in noncentrosymmetric superconductors, the coherence peak of $1/T_1$ is enhanced even for the p -wave pairing dominated states, because of the non-vanishing coherence factor. Thus, from the argument presented in section 3, one possible candidate for the pairing state realized in CePt₃Si is the $s + p$ wave state, in which the p -wave pairing is predominant. The present author and Hayashi et al., independently proposed this pairing state. Furthermore, Hayashi et al. pointed out that in the $s + p$ state, when the magnitude of the s -wave gap Δ_s is close to that of the p -wave gap Δ_p , a line node of the excitation gap appears, because $\Delta_- = \Delta_s - \Delta_p \sin \theta$ can be zero for a specific θ , where θ is the azimuthal angle. Hayashi et al. attributed the line nodes observed at low temperatures in CePt₃Si to this mechanism.²³ This scenario is tempting, since all the experimental observations are explained only by tuning one parameter Δ_s/Δ_p . However, as claimed above, the substantial weight of the s -wave admixture is a bit unlikely in heavy fermion systems in which there is a strong onsite repulsion. The present author proposed another scenario in which the coupling with an antiferromagnetic (AF) order that coexists with the superconductivity in CePt₃Si gives rise to nodal structures of the excitation gap.⁴⁹ The drastic change in the excitation spectrum due to the coexistence of the AF order is not inherent in noncentrosymmetric superconductors, but was pointed out for centrosymmetric conventional

superconductors previously.⁵⁰ In the case of CePt₃Si, the AF order is characterized by the ordering Q -vector along the (001) direction and the staggered moment parallel to the ab -plane.⁹ We demonstrated that for sufficiently large magnitudes of the staggered moment, a line node structure appears in the vicinity of the magnetic Brillouin zone even when the superconducting gap itself has no nodes. Assuming the p -wave pairing state coexisting with the AF order, we calculated the energy dependence of the density of states $D(\varepsilon)$. The results are shown in Fig. 8. Here, m_Q is the magnitude of the staggered moment. In the calculation, we assumed the Rashba type SO interaction, and the \mathbf{d} -vector is $\mathbf{d} = (k_y, -k_x, 0)$. At sufficiently low energies, $D(\varepsilon) \propto \varepsilon$ holds; a characteristic of line nodes. In this calculation, it is assumed that the staggered moment is aligned parallel to the (100) direction. In Fig. 9, we show a schematic figure of the line node structure of the Fermi surface. As a matter of fact, this node structure is not a true node, but a minimum of the excitation gap. Thus, the coherence factor is not suppressed by this node structure, which is in accordance with the existence of the coherence peak of $1/T_1$. It is noted that the node structure has C_{2v} symmetry in momentum space because the direction of the staggered moment breaks C_{4v} symmetry. The experimental detection of this two-fold symmetry is a crucial test for this scenario.

The possibility of the realization of the $s + p$ wave state should be examined by microscopic calculations. For CePt₃Si that has a tetragonal crystal structure with C_{4v} symmetry, basis functions for the s -wave states corresponding to the irreducible representations for A_{1g} are 1, $\cos k_x + \cos k_y$, and $\cos k_z$, as clarified by Sergienko and Curnoe.¹⁸ Thus, a possible candidate for the gap function is given by eq.(14) with $\Delta_s(k) = \Delta_s^{(0)} + \Delta_s^{(1)}(\cos k_x + \cos k_y) + \Delta_s^{(2)}\cos k_z$, $\Delta_t(k) = \Delta_t^{(0)} + \Delta_t^{(1)}(\cos k_x + \cos k_y) + \Delta_t^{(2)}\cos k_z$, and the Rashba type $\mathcal{L}(k) = (\sin k_y, -\sin k_x, 0)$. Even for this gap function, since the isotropic s -wave component $\Delta_s^{(0)}$ is generally nonzero, and gives rise to the coupling with the strong repulsive onsite interaction, its stability should be examined by model calculations. Unfortunately, it is difficult to construct a reliable microscopic model for CePt₃Si at the present moment, since experimental studies of microscopic electronic structure such as the de Haas-van Alphen effect have not yet succeeded in detecting the Fermi surface of heavy electrons in CePt₃Si.³⁵ Very recently, Yanase and Sigrist have carried out microscopic calculations using the Fermi surface obtained by the LDA calculation, and found that the admixture of a p -wave state and an extended s -wave state is stabilized.⁵¹

6. Concluding Remarks

In this review, we survey our theoretical understanding of the unique properties of noncentrosymmetric superconductors. One of the main conclusions is that the remarkable effects due to parity-violation are strongly enhanced by electron correlation, and thus may play crucial roles in heavy fermion systems. From this point of view, the recently discovered superconductors without

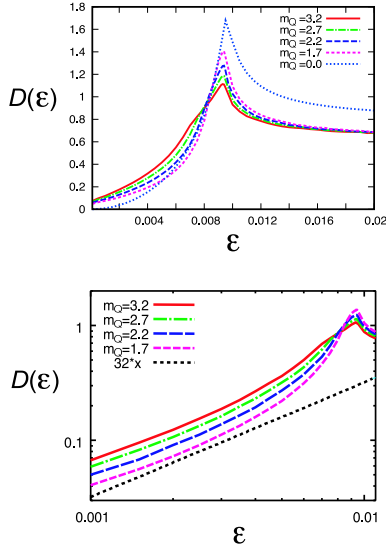


Fig. 8. (Color online) Density of states for p -wave pairing state plotted against excitation energy ε . The upper panel is on a linear scale. The lower panel is a log-log plot.

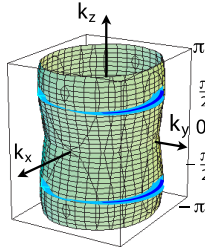


Fig. 9. (Color online) Schematic figure of line node structure on the Fermi surface. The depth of the blue color in the vicinity of the magnetic Brillouin zone $k_z \pm \pi/2$ indicates the depth of the node of the excitation gap.

inversion symmetry such as CePt₃Si, CeRhSi₃, CeIrSi₃, and UIr are quite fascinating systems. It is highly desirable to reveal the interesting features inherent in noncentrosymmetric superconductors experimentally in these novel systems in the near future.

We should note that this review, by no means, encompasses all topics on noncentrosymmetric superconductors. In particular, we could not present arguments on issues on the mixed state in detail. Semiclassical approaches to these subjects have been explored by Hayashi et al. and Nagai et al.^{24, 52} In the case of $\Delta/E_{\text{SO}} \ll 1$ as realized in all heavy fermion superconductors without inversion symmetry, the pairing states on different Fermi surfaces can be approximately separated even under applied magnetic fields, and thus the theoretical treatment is much simplified. However, when $\Delta/E_{\text{SO}} \sim 1$, with finite magnetic fields, the pairing between the different Fermi surfaces can not be negligible, and presumably yields drastic changes of low-energy properties. As a matter of fact, as pointed out recently by Eremin and Annett, the Zeeman field destroys the line node structure due to the admixture of the s -wave pairing and the p -wave pairing considered by Hayashi et al.²³ and mentioned in

section 5, leading to a full-gap state.⁵³ The theoretical clarification of orbital effects in such cases is an interesting future issue.

Acknowledgments

The author is grateful to K. Yamada, Y. Onuki, M. Sigrist, S. K. Yip, D. Agterberg, Y. Matsuda, T. Shibauchi, N. Kimura, T. Takeuchi, R. Settai, M. Ichioka, Y. Yanase, H. Mukuda, M. Yogi, and H. Ikeda for valuable discussions. This work was partly supported by a Grant-in-Aid from the Ministry of Education, Culture, Sports, Science and Technology, Japan.

- 1) V. M. Edelstein: Sov. Phys. JETP **68** (1989) 1244.
- 2) V. M. Edelstein: Phys. Rev. Lett. **75** (1995) 2004.
- 3) V. M. Edelstein: J. Phys. Condens. Matter **8** (1996) 339.
- 4) L. N. Bulaevskii, A. A. Guseinov, and A. I. Rusinov: Sov. Phys. JETP **44** (1976) 1243. In this paper, although the large Pauli limiting field is predicted for the Rashba model, the formulae for the Pauli limiting field, and the spin susceptibility are, unfortunately, not correct.
- 5) L. P. Gor'kov and E. Rashba: Phys. Rev. Lett. **87** (2001) 037004.
- 6) S. K. Yip: Phys. Rev. B **65** (2002) 144508.
- 7) E. Bauer, G. Hilscher, H. Michor, Ch. Paul, E. W. Scheidt, A. Gribanov, Yu. Seropegin, H. Noël, M. Sigrist, and P. Rogl: Phys. Rev. Lett. **92** (2004) 027003.
- 8) T. Takeuchi, S. Hashimoto, T. Yasuda, H. Shishido, T. Ueda, M. Yamada, Y. Obiraki, M. Shiimoto, H. Kohara, T. Yamamoto, K. Sugiyama, K. Kindo, T. D. Matsuda, Y. Haga, Y. Aoki, H. Sato, R. Settai, and Y. Onuki: J. Phys.: Condens. Matter **16** (2004) L333.
- 9) N. Metoki, K. Kaneko, T. D. Matsuda, A. Galatanu, T. Takeuchi, S. Hashimoto, T. Ueda, R. Settai, Y. Onuki, and N. Bernhoeft: J. Phys.: Condens. Matter **16** (2004) L207.
- 10) H. Yasuda, H. Shishido, T. Ueda, S. Hashimoto, R. Settai, T. Takeuchi, T. D. Matsuda, Y. Haga, and Y. Onuki: J. Phys. Soc. Jpn. **73** (2004) 1657.
- 11) M. Yogi, Y. Kitaoka, S. Hashimoto, T. Yasuda, R. Settai, T. D. Matsuda, Y. Haga, Y. Onuki, P. Rogl, and E. Bauer: Phys. Rev. Lett. **93** (2004) 027003.
- 12) M. Yogi, H. Mukuda, Y. Kitaoka, S. Hashimoto, T. Yasuda, R. Settai, T. D. Matsuda, Y. Haga, Y. Onuki, P. Rogl, and E. Bauer: J. Phys. Soc. Jpn. **75** (2006) 013709.
- 13) K. Izawa, Y. Kasahara, Y. Matsuda, K. Behnia, T. Yasuda, R. Settai, and Y. Onuki: Phys. Rev. Lett. **94** (2005) 197002.
- 14) I. Bonalde, W. Brämer-Escamilla, and E. Bauer: Phys. Rev. Lett. **94** (2005) 207002.
- 15) P. A. Frigeri, D. F. Agterberg, A. Koga, and M. Sigrist: Phys. Rev. Lett. **92** (2004) 097001.
- 16) K. Samokhin: Phys. Rev. B **70** (2004) 104521.
- 17) K. V. Samokhin, E. S. Zijlstra, and S. K. Bose: Phys. Rev. B **69** (2004) 094514.
- 18) I. A. Sergienko and S. H. Curnoe: Phys. Rev. B **70** (2004) 214510.
- 19) R. P. Kaur, D. F. Agterberg, and M. Sigrist: Phys. Rev. Lett. **94** (2005) 137002.
- 20) S. K. Yip: J. Low Temp. Phys. **140** (2005) 67.
- 21) K. Samokhin: Phys. Rev. Lett. **94** (2005) 027004.
- 22) S. Fujimoto: Phys. Rev. B **72** (2005) 024515.
- 23) N. Hayashi, K. Wakabayashi, P. A. Frigeri, and M. Sigrist: Phys. Rev. B **73** (2006) 092508.
- 24) N. Hayashi, K. Wakabayashi, P. A. Frigeri, and M. Sigrist: Phys. Rev. B **73** (2006) 024504.
- 25) T. Yokoyama, Y. Tanaka, and J. Inoue: Phys. Rev. B **72** (2006) 220504(R).
- 26) M. Oka, M. Ichioka, and K. Machida: Phys. Rev. B **73** (2006) 214509.
- 27) S. Fujimoto: cond-mat/0605290.
- 28) T. Akazawa, H. Hidaka, H. Kotegawa, T. Kobayashi, T. Fuji-

- wara, E. Yamamoto, Y. Haga, R. Settai, and Y. Ōnuki: J. Phys. Soc. Jpn. **73** (2004) 3129.
- 29) N. Kimura, K. Ito, K. Saitoh, Y. Umeda, H. Aoki, and T. Terashima: Phys. Rev. Lett. **95** (2005) 247004.
 - 30) I. Sugitani, Y. Okuda, H. Shishido, T. Yamada, A. Thamizhavel, E. Yamamoto, T. D. Matsuda, Y. Haga, T. Takeuchi, R. Settai, and Y. Ōnuki: J. Phys. Soc. Jpn. **75** (2006) 043703.
 - 31) M. Hanawa, J. Yamaura, Y. Muraoka, F. Sakai, and Z. Hiroi: J. Phys. Chem. Solids **63** (2002) 1027.
 - 32) K. Togano, P. Badica, Y. Nakamori, S. Orimo, H. Takeya, and K. Hirata: Phys. Rev. Lett. **93** (2004) 247004.
 - 33) P. Badica, T. Kondo, and K. Togano: J. Phys. Soc. Jpn **74** (2005) 1014.
 - 34) H. Q. Yuan, D. F. Agterberg, N. Hayashi, P. Badica, D. Vandervelde, K. Togano, M. Sigrist, and M. B. Salamon: Phys. Rev. Lett. **97** (2006) 017006.
 - 35) S. Hashimoto, T. Yasuda, T. Kubo, H. Shishido, T. Ueda, R. Settai, T. D. Matsuda, Y. Haga, H. Harima, and Y. Ōnuki: J. Phys.: Condens. Matter **16** (2004) L287.
 - 36) N. Kimura, Y. Umeda, T. Asai, T. Terashima and H. Aoki: Physica B294-295 (2001) 280.
 - 37) K. -W. Lee and W. E. Pickett: Phys. Rev. B **72** (2005) 174505.
 - 38) E. I. Rashba: Sov. Phys. Solid State **2** (1960) 1109.
 - 39) G. Dresselhaus: Phys. Rev. **100** (1955) 580.
 - 40) M. I. D'Yakonov and V. I. Perel: Sov. Phys. JETP **33** (1971) 1053.
 - 41) E. A. de Andrada e Silva: Phys. Rev. B **46** (1992) 1921.
 - 42) N. Kimura: presented at International Conference on Magnetism, 2006.
 - 43) L. S. Levitov, Yu. V. Nazarov, and G. M. Eliashberg: Sov. Phys. JETP **61** (1985) 133.
 - 44) V. M. Edelstein: Solid State Commun. **73** (1990) 233.
 - 45) Note that even when the odd parity state is dominant in the noncentrosymmetric superconductor, the Josephson current can flow between this system and a conventional s-wave superconductor, as elucidated by Geshkenbein and Larkin [V. B. Geshkenbein and A. I. Larkin: JETP Lett. **43** (1986) 395].
 - 46) R. Karplus and J. M. Luttinger: Phys. Rev. **95** (1954) 1154; J. M. Luttinger, Phys. Rev. **112** (1958) 739.
 - 47) T. Takeuchi, M. Tsujino, T. Yasuda, S. Hashimoto, R. Settai, and Y. Onuki: J. Magn. & Magn. Mater. to appear.
 - 48) More precisely, the symmetry of $\mathcal{L}_0(k)$ for general k away from the Γ point is lower than the point group symmetry, and thus $\mathcal{L}_0(k)$ for general k should be determined only by microscopic first principle calculations such as the LDA.
 - 49) S. Fujimoto: J. Phys. Soc. Jpn. **75** (2006) 083704.
 - 50) K. Machida, K. Nokura, and T. Matsubara: Phys. Rev. B **22** (1980) 2307; K. Machida: J. Phys. Soc. Jpn. **50** (1981) 2195.
 - 51) Y. Yanase and M. Sigrist: in preparation for publication.
 - 52) Y. Nagai, Y. Kato, and N. Hayashi: J. Phys. Soc. Jpn. **75** (2006) 043706.
 - 53) I. Eremin and J. F. Annett: cond-mat/0606149.